Chin. J. Astron. Astrophys. Vol. 1, No. 3, (2001) 221–235
(*http://www.chjaa.org* or *http://chjaa.bao.ac.cn*)

Chinese Journal of Astronomy and Astrophysics

Soft X-ray Properties of Ultraluminous IRAS Galaxies

Xiao-Yang Xia[1,2] ⋆, Th. Boller[3], Zu-Gan Deng[4,2], G. Börner[5]

[1] Department of Physics, Tianjin Normal University, Tianjin 300074
[2] Beijing Astronomical Observatory and Beijing Astronomical Center of the National Astronomical Observatories, Chinese Academy of Sciences, Beijing 100012
[3] Max-Planck-Institut für Extraterrestrische Physik, Postfach 1312 D-85741 Garching, Germany
[4] Department of Physics, Graduate School, Chinese Academy of Sciences, Beijing 100039
[5] Max-Planck-Institut für Astrophysik, Karl-Schwarzschchild-Straße 1, D-85740 Garching, Germany

Received 2001 February 27 ; accepted 2001 March 13

Abstract We report on the results of cross-correlation of a sample of 903 Ultraluminous IRAS galaxies (ULIRGs) with the ROSAT-All Sky Survey Bright Source Catalogue and the ROSAT archived pointing observations. The sample of ULIRGs has been compiled from the recently released PSCz redshift survey. In total, 35 ULIRGs are securely detected by the ROSAT All-Sky Survey and pointing observations, five of which are blazars. The statistical properties of these sources in the soft X-ray band are determined and compared with their properties in other wavebands. We find that the ratio of the soft X-ray to the far-infrared flux spans about five orders of magnitude and reaches values of about unity. This ratio is a good indicator of the main energy source of ULIRGs. Those with soft X-ray to far-infrared flux exceeding 0.01 are probably powered by accretion onto central supermassive black holes while those with ratios smaller than 0.001 are probably powered by starbursts or other heating processes, or are Compton thick sources. Some ULIRGs have energy contributions from both. This ratio is low for most ULIRGs and hyperluminous infrared galaxies, which explains their low detection rate by ROSAT and ASCA. We also find that some ULIRGs have a similar soft X-ray luminosity vs. temperature relation to that for groups of galaxies and elliptical galaxies, suggesting a common origin of these systems. Our study also reveals a tight correlation between the hardness ratio and the soft X-ray luminosity for Seyfert 1s/QSOs.

Key words: Infrared: galaxies – X-rays: galaxies – Galaxies: active – Galaxies: Seyfert – Galaxies: interactions

⋆ E-mail: xyxia@bac.pku.edu.cn

1 INTRODUCTION

The Ultraluminous IRAS galaxies (ULIRGs) are an important sample for studying the processes of galaxy merging and formation. There have been many studies of these galaxies in many wavebands (see Sanders & Mirabel 1996 for a review), including the soft X-ray band. In the past ten years observations by ROSAT, ASCA and Bepposax, such as for NGC 3690 (Zezas et al. 1998), NGC 6240, Mrk 231, Mrk 273, Arp 220 (Iwasawa & Comastri 1998; Iwasawa 1999; Vignati et al. 1999), IRAS 19254–7245 (Pappa et al. 2000), IRAS 09140–4109 (Fabian et al. 1994), IRAS 20460+1925 (Ogasaka et al. 1997), and IRAS 23060+0505 (Brandt et al. 1997) have been carried out. These studies are, however, usually restricted to a single galaxy or a small number of ultraluminous or hyperluminous IRAS galaxies (Wilman et al. 1998). Rigopoulou et al. (1996) made a statistical study of the soft X-ray properties for six ULIRGs selected from the IRAS Bright Source Catalogue. More recently, Risaliti et al. (2000) carried out a statistical study in the hard X-ray band for a fairly large sample of luminous IRAS galaxies (including about 20 Ultraluminous IRAS galaxies) based on ASCA and Bepposax observations.

While it has become clear that ULIRGs are strongly interacting or merging (e.g. Clements et al. 1996), or multi-merger systems (Borne et al. 2000), there is still a debate about the dominant power source for their tremendous far infrared luminosity.

For some ULIRGs, the dominant energy source appears to be AGN based on the near-infrared spectral properties (Lutz et al. 1999) or hard X-ray properties (e.g. IRAS 05189–2524 and NGC 6240), however they resemble starburst galaxies in the optical or soft X-ray. On the other hand, some ULIRGs are classified as Seyfert 1s /QSOs based on their optical spectra, but they are X-ray quiet and both their soft and hard X-ray properties do not resemble typical optically-selected Seyfert 1s / QSOs (e.g. Mrk 231 and IRAS 07598+6508, see Lawrence et al. 1997; Lipari 1994; Lipari et al. 1994).

The debate about the dominant power source in the object itself hints that star formation and the AGN phenomenon probably occur at the same time. This implies that galaxy formation and the formation and fueling of black holes (BHs) are closely coupled. This is also supported by the prevalence of BHs in nearby galaxies (Magorrian et al. 1998). The implementation of this coupling in semi-analytical studies can explain many properties of quasars (e.g. Kauffmann & Haehnelt 2000). It is therefore interesting to explore the relative contribution of starbursts and AGNs in another part of the energy-spectrum, the soft X-rays.

In the past, many authors have considered the multiple-merger process (e.g. Mamon 1987; Barnes 1985; Barnes 1988, 1999; Schweizer 1989; Weil & Hernquist 1996). Recent high resolution images of ULIRGs from HST lend support to this scenario since many ULIRGs have multi-nuclei and may have resided in compact groups (Borne et al. 2000). The so-called over-luminous elliptical galaxies have X-ray properties similar to groups of galaxies (Ponman et al. 1994; Mulchaey & Zabludoff 1999; Vikhlinin et al. 1999), and may also have formed in multi-merging processes.

The soft X-ray emission in normal elliptical galaxies is assumed to be from hot gas left over from heating processes during their formation or from hot gas expelled from evolving stars (e.g. Mathews & Brighenti 1998). Since most ULIRGs are merging systems and some of these are at the final stage of forming ellipticals (Zheng et al. 1999), it is interesting to compare their soft X-ray properties with those of normal elliptical galaxies and groups of galaxies.

From all the above considerations, ULIRGs are an important (local) sample to study the

connections between galaxy merging, the formation of elliptical galaxies, and the active galactic nuclei (AGNs).

In this paper, we will discuss the properties in soft X-ray band for the largest ULIRG sample based on the PSCz catalogue; we use the X-ray data from ROSAT All Sky Survey and pointing observations, and ASCA observations. The outline of the paper is as follows, in Sect. 2, we discuss how our ULIRG sample is obtained, and the procedure used to identify the X-ray luminous ULIRGs in the ROSAT data. In Sect. 3, we discuss the statistical properties of our sample, and finally in Sect. 4, we summarize and discuss our results. Throughout this paper, we assume an Einstein-de Sitter ($\Omega_0 = 1$) cosmology and adopt $H_0 = 50\,\mathrm{km\,s^{-1}Mpc^{-1}}$.

2 SAMPLE SELECTION

2.1 The ULIRG Sample

The sample of ULIRGs was compiled from the PSCz redshift survey (Saunders et al. 2000). The PSCz catalogue is a complete galaxy redshift survey selected mainly from the IRAS Point Source Catalogue. It includes 15411 IRAS galaxies across 84% of the sky. The PSCz redshift survey is complete down to a flux limit $f_{60\mu\mathrm{m}}$ of 0.6 Jy and $b_j < 19.5^{\mathrm{m}}$. This catalogue is complete and uniform to a few percent at high latitudes and 10% at low latitudes. The PSCz catalogue includes the galaxies from the QDOT survey (Lawrence et al. 1999) and the 1.2 Jy sample (Fisher et al. 1995).

In the adopted cosmology, we find that 903 objects have far-infrared luminosities $L(40 - -120\mu\mathrm{m}) > 10^{12}L_{\odot}$, and hence qualify as ULIRGs according to the criterion of Sanders & Mirabel (1996). This is currently the largest complete sample of ULIRGs. We will correlate this sample with X-ray data as described below.

2.2 The X-ray Sample

There are three catalogues of ROSAT archival data. The first is the ROSAT All Sky Survey Bright Source Catalogue (RASS-BSC, Voges et al. 1999). The RASS-BSC contains 18811 sources and the sky coverage is 92%. Sources in RASS-BSC were detected to a limiting count rate of 0.05 count $\mathrm{s^{-1}}$ in the 0.1–2.4 keV energy band with at least 15 source counts and a detection likelihood of at least 15 (for a definition of likelihood, see Cruddace et al. 1988).

The public PSPC and HRI catalogues contain 74 301 and 59 911 targets, respectively. All three catalogues give source coordinates, count rate, exposure time, hardness ratio and other useful parameters.

2.3 Identifying X-ray Emitting ULIRGs

We have correlated the ULIRGs sample obtained from the PSCz catalogue with the RASS-BSC catalogue and the ROSAT pointing observations from both PSPC and HRI. The details now follow.

First, we correlate the positions of the ULIRGs with those of the RASS-BSC sources and archived ROSAT pointing PSPC and HRI observations resulting in a list of candidate identifications. The largest difference allowed between the soft X-ray and the infrared positions is 36 arcseconds. For two objects (IRAS 10026+4347 and IRAS 18216+6418), the offset is about 36 arcseconds in one observational run, but less than 20 arcseconds in another run. Moreover, for 90% of the targets, the differences between the infrared position and the position given in the ROSAT archive catalogues are about or much less than 20 arcseconds, which is roughly the

pointing uncertainty of the ROSAT PSPC detector. Note that if both ULIRGs and RASS-BSC sources are randomly distributed over all the sky, the expected number of pairs of sources that are within 36 arcseconds of each other is only 0.1, so clearly most of our sources are not due to chance alignment; nevertheless, we take additional steps to ensure secure identifications.

We examine visually by overlaying the X-ray emission contours on optical images from the Palomar Digitized Sky Survey for RASS-BSC identified objects. For a secure identification, the X-ray emission must be spatially coincident with an optical counterpart of the IRAS galaxy. The procedure is the same as in Boller et al. (1998) except that we use the RASS-BSC catalogue instead of the RASS II catalogue and apply a higher detection threshold (15 source counts compared to 6 source counts used by Boller et al.). For pointing source identification, we examine the X-ray image visually and make sure that the PSCz position is coincident with the X-ray image. In addition, we only retain a source if the X-ray source count is larger than 15. There are 19 and 26 identified ULIRGS from the RASS-BSC and the pointing observations, respectively. Taking into account the overlapping sources, there are 35 ULIRGs securely detected by the ROSAT observations.

The basic parameters for the RASS-BSC and the secure pointing identifications are given in Tables 1 and 2, respectively. Many of the X-ray properties of these sources are already available from the ROSAT archives.

Table 1 The Position and Infrared Properties of ULIRGs Detected by ROSAT RASS

(1)	(2)	(3)	(4)	(5)	(6)	(7)	(8)	(9)	(10)
Name	PSCz Position		ROSAT Position		f_{12}	f_{25}	f_{60}	f_{100}	$\Delta\theta$
	α_{2000}	δ_{2000}	α_{2000}	δ_{2000}			[Jy]		arcsec
IR 01268–5436	22.19971	–54.35622	22.19500	–54.35528	0.31	0.42	1.79	2.63	10.44
3C 48⋆,†	24.41767	33.15616	24.42375	33.15875	0.25	0.25	0.79	1.07	20.56
PG 0157+001⋆	29.96033	0.39420	29.96083	0.39361	0.25	0.63	2.34	2.29	2.78
IR 03335+4729	54.26383	47.64796	54.26625	47.64778	0.24	0.62	1.04	1.72	5.90
IR 04505–2958⋆	73.12400	–29.89221	73.12666	–29.89139	0.34	0.19	0.67	1.00	8.81
IR 05494+6058	88.50646	60.97753	88.50708	60.97625	0.25	0.25	1.75	1.98	4.73
IR 06269–0543	97.35233	–5.75776	97.35458	–5.75986	0.23	0.94	3.11	2.83	11.05
OJ +287⋆⋆,†	133.71042	20.10804	133.71458	20.11292	0.35	0.71	0.78	1.13	22.50
IR 10026+4347⋆	151.43124	43.54250	151.42583	43.54556	0.38	0.34	0.62	1.00	17.91
NGC 3690⋆⋆	172.12860	58.56215	172.13126	58.56194	4.01	23.93	119.67	118.58	5.05
IR 11598–0112	180.61012	–1.48729	180.61209	–1.48556	0.36	0.54	2.41	2.72	9.44
3C 273⋆⋆,†	187.27509	2.05309	187.27708	2.05306	0.52	0.93	2.22	2.91	7.16
IR 12442+4550	191.63687	45.57481	191.63876	45.57264	0.26	0.25	0.74	1.09	9.15
IR 15069+1808	227.30792	17.95159	227.30833	17.95361	0.25	0.25	0.74	0.88	7.41
3C 345⋆⋆,†	250.75262	39.80837	250.74544	39.80625	0.32	0.27	0.69	1.07	21.27
NGC 6240⋆⋆	253.24426	2.40101	253.24124	2.39806	0.66	3.60	22.54	27.29	15.19
IR 18216+6418⋆⋆	275.47687	64.34031	275.48917	64.34750	0.19	0.40	1.13	2.16	32.21
IR 20520–2329	313.74100	–23.30713	313.74002	–23.30486	0.25	0.33	0.80	1.62	8.79
IR 23411+0228	355.91370	2.75091	355.91251	2.74583	0.25	0.51	2.35	1.87	18.78

ULIRGs selected from PSCz Redshift Survey Catalogue and ROSAT All-Sky Survey Bright Source Catalogue. Column 1 gives the object name in the IRAS Faint Source Catalogue or the name given in the NED database. The PSCz position and the RASS-BSC position (in degrees) are listed in columns 2 to 5. Columns 6 to 9 give the IRAS fluxes in the 12, 25, 60 and 100μm bands. The differences between the PSCz and RASS-BSC positions are listed in column 10. Objects with ⋆ or ⋆⋆ were also detected by ROSAT PSPC or by both PSPC and HRI (see Tables 2 and 4). Objects with a † sign are blazars.

Table 2 The Position and Infrared Properties Detected in ROSAT Pointings

(1)	(2)	(3)	(4)	(5)	(6)	(7)	(8)	(9)	(10)	(11)
Name	PSCz position		ROSAT Position		z	$f(12)$	$f(25)$	$f(60)$	$f(100)$	$\Delta\theta$
	α_{2000}	δ_{2000}	α_{2000}	δ_{2000}				[Jy]		arcsec
IR 00275–2859	7.51421	–28.70907	7.50667	–28.70728	0.2790	0.260	0.250	0.690	1.200	24.66
3C 48†	24.41767	33.15616	24.42250	33.16031	0.3662	0.25	0.25	0.79	1.07	20.86
PG 0157+001	29.96033	0.39420	29.96042	0.39283	0.1630	0.250	0.625	2.339	2.291	4.94
IR 04505–2958	73.12400	–29.89221	73.12458	–29.89167	0.2852	0.34	0.19	0.67	1.00	2.66
IR 05189–2524	80.25459	–25.36249	80.25542	–25.36008	0.0426	0.701	3.273	13.187	11.995	9.09
IR 07598+6508	121.12671	64.99766	121.12542	64.99650	0.1480	0.264	0.534	1.692	1.730	4.61
OJ +287⋆,†	133.71042	20.10804	133.70583	20.10983	0.3062	0.35	0.71	0.78	1.13	16.80
UGC 5101	143.96471	61.35317	143.96542	61.35639	0.0390	0.296	1.197	12.078	20.417	11.66
IR 10026+4347	151.43124	43.54250	151.42708	43.55194	0.1780	0.380	0.330	0.610	1.000	35.67
IR 10479–2808	162.57663	–28.39936	162.57000	–28.40128	0.1900	0.770	0.360	0.980	1.720	22.10
NGC 3690⋆	172.12860	58.56215	172.13249	58.56439	0.0103	4.008	23.933	119.674	118.577	10.88
3C273⋆,†	187.27509	2.05309	187.27625	2.05114	0.1583	0.517	0.929	2.218	2.911	8.17
Mrk 231⋆	194.05788	56.87379	194.05708	56.87100	0.0422	1.872	8.662	31.99	30.290	10.17
Mrk 273⋆	206.17488	55.88688	206.17208	55.88442	0.0378	0.235	2.282	21.74	21.38	10.51
PKS 13451+1232	206.89017	12.29019	206.88667	12.28758	0.1202	0.143	0.669	1.916	2.060	15.49
IR 14348–1447	219.40512	–15.00645	219.40458	–15.00833	0.0823	0.140	0.495	6.870	7.068	7.02
IR 15033–4333	226.68076	–43.74525	226.68208	–43.74131	0.0966	0.155	0.309	2.258	4.889	14.59
Arp 220⋆	233.73575	23.50370	233.73728	23.50243	0.0177	0.647	8.110	107.399	118.304	6.81
3C 345⋆,†	250.75262	39.80837	250.74542	39.80875	0.5922	0.32	0.27	0.69	1.07	19.96
NGC 6240⋆	253.24426	2.40101	253.24506	2.40049	0.0243	0.656	3.597	22.542	27.290	3.43
IR 16541+5301	253.83241	52.94181	253.83500	52.94272	0.1940	0.250	0.250	0.700	1.700	6.50
IR 18216+6418⋆	275.47687	64.34031	275.48708	64.34175	0.297	0.19	0.40	1.13	2.16	16.74
IR 20551–4250	314.61374	–42.64979	314.61208	–42.64672	0.0428	0.284	1.906	12.78	9.948	11.89
IR 21219–1757	321.17258	–17.74612	321.17292	–17.74094	0.1103	0.290	0.410	1.140	1.260	18.68
3C 446†	336.44263	–4.95377	336.44750	–4.95289	1.4041	0.46	0.36	0.67	1.00	17.75
IR 22491–1808	342.95712	–17.87291	342.95375	–17.87194	0.0778	0.250	0.569	5.536	4.645	12.06

The object name as given in the IRAS Faint Source Catalogue or in the NED is listed in Column 1. The PSCz and ROSAT positions (in degrees) are given in columns 2 to 5. Column 6 lists the redshifts of the object. The 12, 25, 60, and 100μm fluxes are given in column 7 to 10. The differences between the PSCz and ROSAT PSPC positions are listed in columns 11. Objects with ⋆ were detected by both PSPC and HRI. Objects with a † sign are blazars.

To obtain further properties (such as their spectral and spatial behaviors and model-dependent soft X-ray luminosities), we have analyzed the X-ray data based mainly on the PSPC and HRI observations using the EXSAS software at MPE. For point sources with detected photons larger than 100, we have performed spectral fitting and also tested for variability (see Sect. 3.5). The best spectral fitting results are listed in Table 4. For extended sources with enough detected photons, such as NGC 3690, NGC 6240, Mrk 273 and Arp 220, we perform a spectral analysis based on the PSPC data and a spatial analysis based on the HRI data. Our results for these 4 sources generally agree with their previously published results (e.g. Iwasawa 1999; Fricke & Papaderos 1998; Schulz et al. 1998), and so will not be shown here.

3 STATISTICAL RESULTS

The main X-ray properties of the secure identifications with the RASS-BSC are presented in Table 3, together with their far-infrared properties. Table 4 lists the basic X-ray and other waveband properties for the ROSAT pointing identifications. For objects with more than 100 source photons (cf. column 4 in Table 4), the X-ray spectral properties have been derived from a power-law fit with free spectral index and absorbing column density. The absorption is required to be at least as large as the Galactic value taken from Stark et al. (1992) (these cases have error bars in the $N_{\rm Hfit}$ value at column 6 of Table 4); for IR 10026+4347, we use $\Gamma = 3.2$ and $N_{\rm Hfit} = (2.3 \pm 1.3) \times 10^{20}{\rm cm}^{-2}$ from the RASS data fitting result (Xia et al. 1999).

For objects with less than 100 source photons we use a simple power-law model, with the photon index fixed at $\Gamma = 2.3$ (which is typical for extragalactic objects discovered by ROSAT, see Voges et al. 1999), and an absorption column density $N_{\rm Hgal}$ of hydrogen fixed at the Galactic value along the line of sight.

Table 3 Soft X-ray Properties of ULIRGs Detected by ROSAT RASS

(1) Name	(2) Count Rate [counts s^{-1}]	(3) Expo [s]	(4) $N_{\rm ph}$	(5) $N_{\rm Hgal}$ [10^{21}]	(6) z	(7) $\log L_{\rm X}$ [erg s^{-1}]	(8) $\log L_{\rm FIR}$ [erg s^{-1}]	(9) $L_{\rm X}/L_{\rm FIR}$	(10) HR	(11) Class
IR 01268–5436	0.497±0.110	46	23	0.224	0.0929	44.53	45.73	6.31e–2	–0.10	Sy 1
3C 48†	0.646±0.044	352	227	0.452	0.3662	45.63	46.57	1.15e–1	0.21	QSO
PG 0157+001	0.208±0.026	401	83	0.251	0.1630	44.37	46.08	1.95e–2	–0.08	QSO
IR 03335+4729	0.099±0.016	493	49	4.471	0.1828	45.26	46.09	1.48e–1	0.92	Sy 1
IR 04505–2958	0.213±0.002	374	80	0.180	0.2852	44.71	46.28	2.69e–2	–0.71	QSO
IR 05494+6058	0.042±0.011	366	15	1.050	0.0910	43.88	45.46	2.63e–2	0.96	Sy 1.8
IR 06269–0543	0.132±0.018	513	68	4.250	0.1171	44.97	46.08	7.76e–2	1.00	1Zw1
OJ +287◇	0.164±0.024	320	52	0.305	0.3062	44.92	46.41	3.24e–2	0.32	BL Lac
IR 10026+4347	0.668±0.039	508	339	0.108	0.1780	45.38	45.84	3.47e–1	–0.61	QSO
NGC 3690	0.109±0.017	524	57	0.106	0.0103	41.73	45.39	2.19e–4	0.78	HII
IR 11598–0122	0.097±0.019	256	25	0.226	0.1507	44.32	46.04	1.91e–2	–0.77	Sy 1
3C 273†	7.044±0.390	366	2578	0.179	0.1583	46.07	46.07	0.00e0	–0.04	QSO
IR 12442+4550	0.075±0.015	488	37	0.152	0.1965	44.45	45.99	2.88e–2	–0.62	Sy 1
IR 15069+1808	0.082±0.002	364	30	0.255	0.1699	44.35	45.82	3.39e–2	–0.22	Sy 1
3C 345†	0.323±0.026	616	199	0.101	0.5922	45.76	46.98	6.03e–2	–0.18	QSO
NGC 6240	0.035±0.008	507	18	0.549	0.0240	42.03	45.43	3.98e–4	0.97	LINER
IR 18216+6418	1.070±0.014	5257	5625	0.424	0.297	45.79	46.59	1.58e–1	0.24	QSO
IR 20520–2329	0.099±0.001	432	43	0.515	0.2053	44.89	46.12	5.89e–2	0.02	Sy 1
IR 23411+0228	0.057±0.015	373	21	0.445	0.0908	43.74	45.72	1.05e–2	0.06	Sy 1

Object names, RASS count rate (or reduced count rate), the RASS exposure time, and the number of source photons are given in columns 1 to 4, respectively. The Galactic absorption column density of neutral hydrogen taken from Stark et al. (1992) is given in column 5. The redshift is given in column 6. The 0.1−2.4 keV and the 40–120μm luminosities are listed in columns 7 and 8 , respectively. The luminosity ratios in these two bands are at column 9. Column 10 lists the hardness ratios from ROSAT All Sky Survey Bright Source Catalogue and the optical classifications from the literature are in Column 11. Objects with a † sign are blazars.

Table 4 Soft X-ray and Other Waveband Properties of ULIRGs Detected by ROSAT Pointings

(1)	(2)	(3)	(4)	(5)	(6)	(7)	(8)	(9)	(10)	(11)	(12)	(13)
Name	Count Rate [counts s^{-1}]	Expo [s]	N_{phot}	N_{Hgal} [10^{20} cm^{-2}]	N_{Hfit}	Γ	log L_X	log L_{FIR} [erg s^{-1}]	log L_K	L_X/L_{FIR}	HR	Class
IR 00275–2859	0.006±0.008	4497	51	1.90	1.90	2.3±0.0	43.41	46.30	–	1.29e–3	–0.34	QSO
3C 48†	0.298±0.003	5577	1662	4.52	3.25 ±1.16	2.4±0.3	45.29	46.57	–	5.25e–2	0.33	QSO
PG 0157+001	0.204±0.006	6155	1255	2.51	4.55 ±0.95	3.1±0.2	44.36	46.08	44.82	1.91e–2	–0.16	QSO
IR 04505–2958	0.283±0.002	3422	969	1.80	1.40±0.46	3.0±0.2	44.83	46.28	–	3.55e–2	–0.58	QSO
IR 05189–2524	0.035±0.003	4371	152	1.93	1.93	2.4±0.2	42.37	45.65	44.21	5.25e–4	–0.12	Sy2
IR 07598+6508	0.002±0.001	8207	20	4.35	4.35	2.3±0.0	42.84	45.86	45.23	9.55e–4	0.72	QSO
OJ +287◇	0.272±0.009	3605	981	3.05	2.86±0.86	2.2±0.3	45.14	46.41	–	5.37e–2	0.34	BL Lac
UGC 5101	0.004±0.001	17322	73	2.54	2.54	2.3±0.7	41.72	45.82	43.90	7.94e–5	0.58	LINER
IR 10026+4347	0.085±0.073	949	81	1.08	2.28±1.30	3.2±0.5	44.49	45.84	–	4.47e–1	–0.58	QSO
IR 10479–2808	0.011±0.001	6681	71	5.08	5.08	2.3±0.0	43.86	46.11	–	5.62e–3	0.76	QSO
NGC 3690	0.089±0.004	6391	568	1.06	5.64±1.66	2.2±0.4	41.68	45.39	43.44	1.95e–4	0.69	HII
3C 273†	6.454±0.032	6140	39627	1.79	1.87±0.01	2.0±0.1	46.03	46.06	45.59	9.33e–1	–0.01	QSO
Mrk 231	0.014±0.001	23930	335	1.29	4.20±2.54	2.5±0.7	42.09	46.04	44.79	1.12e–4	0.36	Sy1
Mrk 273	0.013±0.001	20671	270	1.05	9.45±5.89	3.3±1.1	41.92	45.78	44.21	1.38e–4	0.34	Sy2
PKS 13451+1232	0.004±0.001	3793	15	1.86	1.86	2.3±0.0	42.63	45.74	44.15	7.76e–4	0.58	Sy2
IR 14348–1447	0.004±0.001	4781	20	7.78	7.78	2.3±0.0	42.67	45.96	44.09	5.13e–4	1.0	LINER
IR 15033–4333	0.002±0.001	6615	15	8.07	8.07	2.3±0.0	42.55	45.73	–	6.61e–4	0.0	–
Arp 220	0.009±0.001	22485	193	4.30	8.32±5.65	2.7±1.0	41.06	45.83	43.93	1.70e–5	0.72	Sy2
3C 345†	0.313±0.013	3899	1220	1.01	1.50±0.62	2.0±0.3	45.75	46.98	–	5.89e–2	0.04	QSO
NGC 6240	0.064±0.003	5232	337	5.49	5.49	1.5±0.2	42.29	45.43	43.73	7.24e–4	0.91	LINER
IR 16541+5301	0.004±0.001	15390	68	4.09	4.09	2.3±0.0	43.32	46.05	–	1.86e–3	0.88	Sy2
IR 18216+6418	1.259±0.034	17152	21594	4.24	4.24	2.0±0.2	45.86	46.59	–	1.86e–1	0.48	QSO
IR 20551–4250	0.006±0.001	6702	43	3.82	3.82	2.3±0.0	42.11	45.63	–	3.02e–4	0.91	HII
IR 21219–1757	0.018±0.004	1906	35	4.51	4.51	2.3±0.0	43.42	45.60	–	6.61e–3	0.0	QSO
3C 446†	0.088±0.002	15198	1337	5.08	7.15±0.83	2.1±0.2	46.17	47.78	–	2.45e–2	0.80	BL Lac
IR 22491–1808	0.004±0.003	5238	20	2.69	2.69	2.3±0.0	42.33	45.95	43.65	2.40e–4	0.20	HII

Only objects with highly secure identifications are listed. The object name, count rate (or reduced count rate), the exposure time, and the number of source photons are given in columns 1 to 4, respectively. The Galactic absorption column density taken from Stark et al. (1992) is listed in column 5. The absorbing column density in the best power-law model fit is given in column 6 (the values with no error bars are Galactic absorbing column densities). The fit photon index Γ is given in columns 7 (zero error means that we used a simple power-law model, with the photon index fixed at $\Gamma = 2.3$ based on Voges et al. (1999) for objects with less than 100 detected photons.) The modeled soft X-ray luminosities in the 0.1–2.4 keV band and the 40–120 μm band luminosities based on Eq. (7) of Schmidt & Green (1986) are listed in columns 8 and 9, respectively. The K band luminosities from the literature (Surace & Sanders 1999; Surace et al. 2000) are listed in columns 10. The ratios of soft X-ray in the 0.1–2.4 keV band and the far infrared luminosities in the 40–120 μm band are listed in column 11. Column 12 and 13 list the hardness ratios from ROSAT pointing catalogues and optical classifications from the literature. Objects with a † sign are blazars.

The power-law fit is excellent for most Seyfert 1s/QSOs, all of which have a point-like soft X-ray morphology. There are also five bright radio loud QSOs or BL Lac objects in the sample: 3C 48, 3C 273, 3C 345, OJ 287 and 3C 446. To see clearly the effects of these blazars, we show the statistical results with and without these sources.

We also use different models to fit the spectra for objects with extended emission, such as NGC 6240, Mrk 273, NGC 3690 and Arp 220 (Iwasawa 1999). The hot plasma model usually fits better although the power-law fit is also acceptable based on the ROSAT data alone. As the energy resolution of ROSAT is lower than that of ASCA, we shall discuss some correlations based on ASCA results from the literature in Section 3.4.

3.1 The soft X-ray luminosity

In Figure 1, we plot the $L_{\rm X}/L_{\rm FIR}$ as a function of the infrared luminosity. It is clear from this figure (and Tables 3 and 4) that the ratio of the soft X-ray luminosity to the far infrared luminosity of ULIRGs spans about five orders of magnitude and reaches to around unity. If we exclude the five blazars, this range of ratios is about a factor of 3 smaller. Since the ROSAT All Sky Survey has a relatively short exposure time, the sources detected in this survey are mainly soft X-ray luminous objects (the soft X-ray luminosities $\gtrsim 10^{44}{\rm erg\,s^{-1}}$), the exceptions are NGC 3690 and NGC 6240 at very low redshifts.

Further investigation reveals that most RASS sources are Seyfert 1s/QSOs (see column 11 of Table 3). Moreover, some of them are Seyfert 1s/QSOs with extremely strong Fe II emission and their soft X-ray spectrum can be fitted well with very steep power-laws. A good example, IRAS 10026+4347, has been presented in Xia et al. (1999).

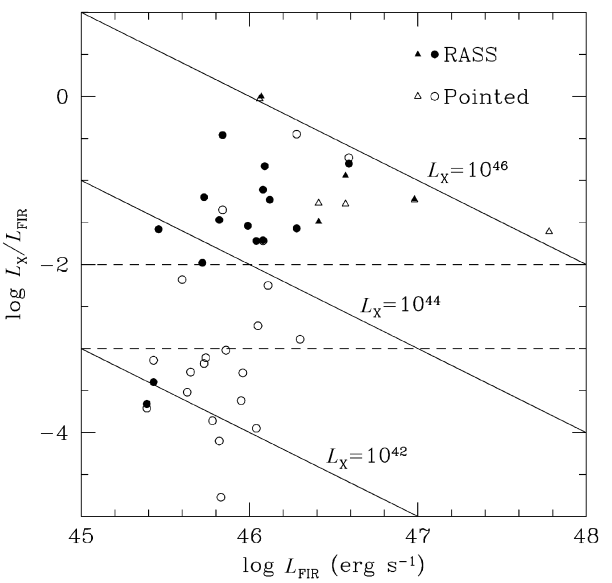

Fig. 1 The ratio of soft X-ray luminosity to infrared luminously vs. infrared luminosity. Open and filled circles are for the RASS-BSC and pointing samples, respectively; the (five) blazars are shown as filled triangles from the RASS-BSC sample and as open triangles from pointing observations. The three solid lines indicate lines with $L_{\rm X} = 10^{42}, 10^{44}, 10^{46}{\rm erg\,s^{-1}}$, respectively. The ULIRGs above the top horizontal dashed line are probably dominated by AGNs while those below the bottom horizontal dashed line are dominated by starbursts. The ULIRGs between these two lines may have contributions from both.

In comparison, for sources detected in pointing observations, the soft X-ray luminosities extend to fainter levels and cover a somewhat broader range. The most luminous objects in the soft X-ray band are Seyfert 1s/QSOs and their soft X-ray emission is mainly from a central AGN. However, some infrared Seyfert 1s/QSOs, such as Mrk 231, IRAS 07598+651 and IRAS 00275–2859, are relatively weak in soft X-rays compared to their far infrared luminosities.

From Figure 1, Table 3 and Table 4, it appears reasonable that those with $L_{\rm X}/L_{\rm FIR} > 0.01$ are dominated by AGNs while those with the ratio smaller than 0.001 are dominated by starbursts, or Compton thick sources; those galaxies in between may have contributions from both. This dichotomy shows up also in the soft X-ray morphologies and the spectra. This result is in good agreement with the hard X-ray statistical results for a luminous IRAS galaxy sample by Risaliti et al. (2000), which includes about 10 objects in our sample.

Since the most X-ray luminous ULIRGs are Seyfert 1s/QSOs and given that fewer than 10% ULIRGs are Seyfert 1s/QSOs (Lawrence et al. 1999), it is easy to understand why the ROSAT detection rate of ULIRGs is very low. Even the most hyperluminous IRAS galaxies are not detected, which yields a mean upper limit of $L_{\rm X}/L_{\rm bol} \lesssim 2.3 \times 10^{-4}$ (Wilman et al. 1998). We will return to the properties of this luminous IRAS Seyfert 1s/QSOs sample in Section 3.5.

3.2 The Correlation with $L_{\rm K}$

We have compiled the K-band luminosities from Surace et al. (2000), and Surace & Sanders (1999) for identified ULIRGs. Their data are listed in Table 4. Most of these galaxies have $L_{\rm X}/L_{\rm FIR} < 10^{-3}$, so their energy budget is probably dominated by starbursts. Figure 2 shows the correlation of soft X-ray luminosities with the luminosities in the K bands for fourteen sources, including one blazer 3C 273. The X-ray luminosity is clearly correlated with the K-band luminosity. Excluding 3C 273, the correlation coefficient is 0.61 with 99.7% significance. Moreover, the scatter for the K-band luminosity for a given $L_{\rm X}$ is only about one order of magnitude. This is in sharp contrast with the large scatter seen in $L_{\rm X}/L_{\rm FIR}$ (see Fig. 1). This relatively tight correlation can be understood as follows.

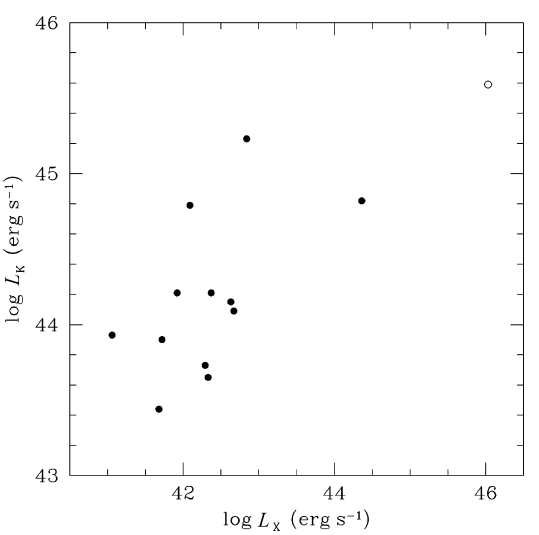

Fig. 2 X-ray luminosity vs. K-band luminosity for the ULIRGs listed in Table 4. The open circle is for the only blazer in the figure, 3C 273.

As discussed by Iwasawa & Comastri (1998), the optical depths at 2.2 μm and the soft X-ray band are similar if the standard gas to dust ratio is assumed and the powerful K band continuum is taken to signify the presence of a large number of red giants and supergiants.

Therefore, the correlation between $L_{\rm X}$ and $L_{\rm K}$ shows that at least a part of the soft X-ray emission in these ULIRGs (mostly with small $L_{\rm X}/L_{\rm FIR}$ ratio) is from starbursts.

3.3 The Hardness Ratio

The hardness ratio is defined as

$$\mathrm{HR} = \frac{f_{0.5-2.0} - f_{0.1-0.4}}{f_{0.5-2.0} + f_{0.1-0.4}}, \tag{1}$$

where $f_{0.5-2.0}$ and $f_{0.1-0.4}$ are the fluxes in the 0.5–2.0 keV and 0.1–0.4 keV ranges, respectively ($-1 \leq \mathrm{HR} \leq 1$). For most of our targets, we obtain the hardness ratio from the RASS-BSC and pointing archive catalogues directly; for the remaining small fraction, we obtain this by spectral fitting. For the overlapping sources between the RASS-BSC sample and pointing observations, we take the hardness ratio from the latter. From the left panel of Fig. 3, it can be seen that there is a weak correlation between the hardness ratio and the soft X-ray luminosity for all our targets. However, for the 16 ULIRGs with $L_{\rm X} > 10^{44}\,\mathrm{erg\ s^{-1}}$, which are mainly Seyfert 1s or QSOs, the correlation is tighter. We find that the correlation coefficient is 0.47 with 93.6% significance. If we exclude the five blazars, the correlation coefficient is 0.43 with 80.4% significance.

This correlation indicates that the Seyfert 1s/QSOs with relatively low soft X-ray luminosities also tend to have very soft X-ray spectra. Given that soft X-ray luminosity is higher in QSOs than in Seyfert 1's, this result is consistent with the scenario where the soft X-ray excess for low-luminosity AGNs is due to the so-called 'Big Blue Bump'; this feature is less prominent for the more luminous QSOs in the soft X-ray and hence their spectra are harder (see Reeves & Turner 2000). We caution, however, that the correlation is not highly significant for the current sample, especially if we exclude the blazars.

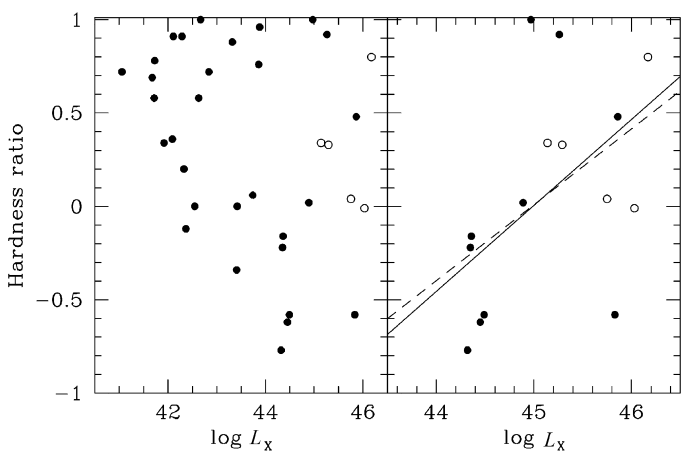

Fig. 3 The left panel shows the hardness ratio (defined in Eq.(1)) vs. $L_{\rm X}$ for the sample with 35 objects; the right panel for objects with $L_{\rm X} > 10^{44}\mathrm{erg\ s^{-1}}$. The open circles mark the five blazars. The solid (dashed) straight line is the best linear regression through the points in the right panel without (with) the five blazars. The ULIRG sample is given in Tables 3 and 4.

3.4 The Hot Gas of ULIRGs

As mentioned above and discussed in detail by Iwasawa (1999), for ULIRGs with relatively low soft X-ray luminosities, the power-law fitting to the soft X-ray spectra is not as good as the hot plasma model fitting. Also, the soft X-ray emissions are extended for these objects from the ROSAT HRI observations. Examples include NGC 3690, NGC 6240, Arp 220 and Mrk 273 (Zezas et al. 1998; Iwasawa 1999).

Because the energy resolution of ROSAT is lower than that of ASCA, we collect the ASCA data in the soft X-ray band for these objects. For objects with enough detected photons to perform the analysis, the two-temperature model provides the best fit to the observational data. Iwasawa (1999) pointed out that the low temperature component is more extended spatially than the high temperature component. He argued that the high temperature component is from a central massive starburst region. Table 5 lists the soft X-ray luminosities and the temperatures available from the hot plasma model fitting. For those fitted with a two-temperature model, we only take the value for the low temperature component since we are interested in the extended emission in the outer region.

Table 5 The Soft X-ray (0.1–2.0 keV) Luminosities and Temperatures

(1)	(2)	(3)	(4)	(5)
Name	$\log L_{\rm X}$ [erg s^{-1}]	T [keV]	Reference	Model
NGC 3690	41.67	0.83±0.03	Zezas et al.	Two Temp. R-S model fit
Mrk 231	41.95	$0.88^{+0.27}_{-0.17}$	Iwasawa	Two Temp. thermal model fit
Mrk 273	41.99	$0.47^{+0.24}_{-0.15}$	Iwasawa	thermal model fit
Arp 220	40.95	$0.76^{+0.13}_{-0.11}$	Iwasawa	thermal model fit
NGC 6240	42.19	$0.60^{+0.07}_{-0.10}$	Iwasawa	Two Temp. thermal model fit
IRAS 19254–7245	41.29	0.8	Pappa et al.	fixed Temp.
IRAS 20460+1925	42.93	1.0	Ogasaka et al.	fixed Temp.
NGC 1132	43.00	1.11±0.02	Mulchaey et al.	R-S model fit
1159+5531	43.34	2.2	Vikhlinin et al.	cluster & group $L_{\rm x}$-T relation
1340+4017	43.40	2.3	Vikhlinin et al.	cluster & group $L_{\rm x}$-T relation
2114-6800	43.30	2.1	Vikhlinin et al.	cluster & group $L_{\rm x}$-T relation
2247+0337	43.61	2.8	Vikhlinin et al.	cluster & group $L_{\rm x}$-T relation

The soft X-ray (0.1–2.0 keV) luminosities and temperatures for ultraluminous IRAS galaxies above the horizontal line and for soft X-ray over-luminous ellipticals (OLEGs) below that line. All data are from the literature and most are based on ASCA observations with high energy resolution. The $L_{\rm X}$-T relation of clusters and groups of galaxies is from Hwang et al. (1999).

For comparison, we also collect the soft X-ray luminosity and temperature data for Hickson compact groups from Ponman et al. (1996) and for elliptical galaxies from Buote & Fabian (1997). The Hickson compact groups data are based on ROSAT PSPC observations and data for elliptical galaxies are based on ASCA observations (the $L_{\rm X}$ is in 0.5–2 keV band). There are also data for 5 soft X-ray over-luminous elliptical galaxies (OLEGs) from Vikhlinin et al. (1999) and Mulchaey & Zabludoff (1999) in Table 5. The temperature of OLEGs by Vikhlinin et al. has been determined from the $L_{\rm X}$-T relation of clusters and groups of galaxies (Hwang et al. 1999).

Figure 4 shows the $L_{\rm X}$ vs. temperature relation for ULIRGs, groups of galaxies, elliptical galaxies and five OLEGs. The most important feature is that the ULIRGs occupy the same

region in the $L_{\rm X}$ and T plane as groups of galaxies and elliptical galaxies. The OLEGs clearly have higher soft X-ray luminosity and temperature than compact groups and elliptical galaxies.

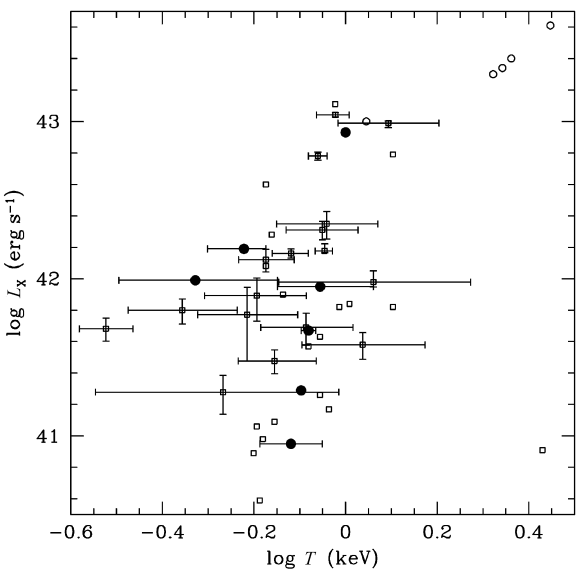

Fig. 4 The soft X-ray luminosity vs. the temperature of the hot gas. The filled circles are for selected ULIRGs. For comparison, we also plot the data for Hickson compact group from Ponman et al. (1996) as open squares and for elliptical galaxies from Buote & Fabian (1998) as solid squares. The five open circles at top right are for overluminous ellipticals from Vikhlinin (1999) and Mulchaey & Zabludoff (1999).

The data therefore indicate that the low temperature component hot gas in ULIRGs may have the same origin as the hot gas in groups of galaxies and elliptical galaxies. Hence it hints at an evolutionary connection between ULIRGs, groups of galaxies and elliptical galaxies.

3.5 Soft X-ray Properties of IRAS Seyfert 1s/QSOs

It is clear from Tables 2 and 3 that about two thirds (22 out of 35) of ROSAT detected ULIRGs are Seyfert 1s/QSOs or BL Lac objects. Given that a large fraction of Seyfert 1s/QSOs selected from ULIRGs are strong or extremely strong optical FeII emitters (Lawrence et al. 1999; Zheng et al. 2000, in preparation), this Seyfert 1s/QSOs sub-sample is suitable for investigating the correlations between the properties of optical emission lines and soft X-rays.

From Tables 3 and 4 we see that most Seyfert 1s/QSOs have a soft X-ray luminosity $L_{\rm X} \gtrsim 10^{44}\,{\rm erg\,s^{-1}}$ and the ratio of soft X-ray to far infrared luminosity is larger than 0.01 with a few exceptions: Mrk 231, IRAS 07598–6508, IRAS 00275–2859, IRAS 21219–1757 and IRAS 10479–2818. All these five objects are QSOs from NED.[1]

[1] The NASA/IPAC Extragalactic Database (NED) is operated by the Jet Propulsion Laboratory, California Institute of Technology, under contract with the National Aeronautics and Space Administration.

Furthermore, four of these five objects (except IRAS 10479–2818) have extremely strong/or very strong FeII emissions. Mrk 231 and IRAS 07598–6508 are broad absorption line quasars. IRAS 10479–2818 is not an FeII emitter and has very broad permitted emission lines (Clowes, Leggett & Savage 1991). However the ratio of Hα to Hβ is much larger than 3.1, the value for normal Seyfert 1s/QSOs, which means that there is heavy absorption in this object. Therefore, the low soft X-ray luminosity for these five IR QSOs is probably due to heavy absorption (see Brandt et al. 2000).

For Seyfert 1s/QSOs with high soft X-ray luminosity and high $L_{\rm X}/L_{\rm FIR}$ ratio, the soft X-ray spectra can be fitted very well by power-laws with spectral index around 2.3 for most of them and these fit the description of classical Seyfert 1s/QSOs. However, for IRAS 10026+4347, IRAS 04505–2958, IRAS 11598–0122 and PG 0157+001, the power-law slopes are steeper with a photon index $\Gamma \gtrsim 3$, or the spectra are very soft (for a power-law spectrum there is a one-to-one correspondence between the hardness ratio and spectral index).

The soft X-ray spectra for the first three objects are very soft as shown in column 13 of Table 4. These three Seyfert 1s/QSOs are also extremely strong or very strong optical FeII emitters. Therefore in their soft X-ray loudness, steep spectral index and strong optical FeII emission they resemble the narrow-line Seyfert 1 galaxies (NLS1, Boller et al. 1996), although their permitted emission line widths for IRAS 10026+4347 and PG 0157+001 are not as narrow as a typical NLS1 – their Hβ widths are larger than 2000 km s^{-1} (Zheng et al. 2000, in preparation). Also comparing the count rate and soft X-ray luminosities in Tables 3 and 4, one clearly sees variability for some of the Seyfert 1s/QSOs. However, the variabilities are up to about a factor of two, except for IRAS 10026–4347, so these ULIRGs may have variabilities between typical NLS1s and normal Seyfert 1s/QSOs.

To summarize, the sub-sample of 22 Seyfert 1s/QSOs exhibit very different properties in their soft X-ray luminosity, spectral slope or hardness ratio, and there does not seem to be a simple correlation with optical spectral properties. Some of the diversity may be caused by large and varying dust obscuration, but some may be intrinsic.

4 SUMMARY AND DISCUSSION

We have correlated a sample of 903 ULIRGs selected from the PSCz IRAS galaxy redshift survey catalogue with the ROSAT All-Sky Survey Bright Source Catalogue and ROSAT PSPC and HRI pointing archival data. The identification of ULIRGs as X-ray emitters is based on X-ray contour plots overlaid on optical images taken from the Digitized Sky Survey or by visual coincidence of the soft X-ray image and the PSCz position. In total, 35 ULIRGs have been securely detected by ROSAT observations, including five blazars.

We have determined the main soft X-ray properties for the identified objects and studied their properties in other wavebands. Our statistical results depend somewhat on whether we include the five blazars or not, but not to a very significant degree. The most striking result is the ratio between the soft X-ray and the far-infrared flux which covers five orders of magnitude, much more than the K-band luminosity to $L_{\rm X}$ ratio.

The highest $L_{\rm X}/L_{\rm FIR}$ ratio is close to one, and these soft X-ray luminous ULIRGs are most likely powered by accretion onto central massive black holes, while the lower ratio systems may be powered by starbursts or Compton thick sources. It is clear that the X-ray energy sources in these ULIRGs may be quite diverse. We also found a correlation between the hardness ratio and the soft X-ray luminosity for 16 ULIRGs with $L_{\rm X} > 10^{44}$erg s^{-1}, which is consistent with

the result for a large QSO sample with ASCA by Reeves & Turner (2000).

Two-thirds of our identified ULIRGs are Seyfert 1s/QSOs, while the remaining one-third are not. For several extended objects that are classiable as Seyfert 1s/QSOs, we use the published ASCA data to study the origin of the hot gas. We find that the hot gas seems to follow the same $L_{\rm X}$ vs. T trend as do groups of galaxies and luminous elliptical galaxies. This suggests that some ULIRGs are evolutionally linked with groups of galaxies and elliptical galaxies. The Seyfert 1s/QSOs in the ULIRGs have different properties, some have relatively weak soft X-ray emission, while others have higher luminosities ($L_{\rm X} > 10^{44}\,{\rm erg\,s^{-1}}$); the latter can be further divided into ones with steep slopes and those with slopes that are typical for classical Seyfert 1s/QSOs. Optical spectra have recently been obtained for this unique sample of Seyfert 1s/QSOs. The results of the analysis will be discussed in detail in a forthcoming paper.

Acknowledgements The authors thank Profs. J. Trümper and L. Z. Fang for stimulating this identification project. We also thank Drs. H. Wu and X. Z. Zheng for reducing the optical spectra of some identified ULIRGs and Profs. X. P. Wu and T. Q. Wang for helpful discussions. XYX and DZG thank the Max-Planck Institute for Astrophysics for hospitality. This research is supported by the National Natural Science Foundation of China, the NSFC-DFG exchange program and the NKBRSF G19990754.

References

Barnes J. E., 1985, MNRAS, 215, 517
Barnes J. E., 1988, ApJ, 331, 699
Barnes J. E., 1989, Nature, 338, 123
Boller Th., Bertoldi F., Dennefeld M., Voges W., 1998, A&AS, 129, 87
Boller Th., Brandt W. N., Fink H., 1996, A&A, 305, 53
Borne K. D., Bushouse H., Lucas R. A., Colina L., 2000, ApJ, 529, L77
Brandt W. N., Fabian A. C., Takahashi K. et al., 1997, MNRAS, 290, 617
Brandt W. N., Boller Th., 1998, Astronomische Nachrichten, 319, 163
Brandt W. N., Laor A., Wills B. J., 2000, ApJ, 528, 637
Buote D. A., Fabian A. C., 1997, MNRAS, 296, 977
Clements D. L., Sutherland W. J., Mcmahon R. G., Saunders W., 1996, MNRAS, 279, 477
Clowes R. G., Leggett S. K., Savage B., 1991, MNRAS, 250, 597
Comastri A., Brandt W. N., Leighly K. M. et al., 1998, A&A, 333, 31
Cruddace R. G., Hasinger G. R., Schmitt J. H. M. M., 1988, In: Murtagh F., Heck A., eds., Astronomy from Large Databases: Scientific Objectives and Methodological Approaches, ESO Press, Garching, p. 177 (ESO Conference and Workshop Proceedings 28)
Fabian A. C., Shioya Y., Iwasawa K. et al., 1994, ApJ, 436, L51
Fisher K. B., Strauss M. A., Davis M., Yahil A., Schlegel D., 1995, ApJS, 100, 69
Fricke K. J., Papaderos P., 1998, astro-ph/9810144
Hwang U., Mushotzky R. F., Burns J. O., Fukazawa Y., White R. A., 1999, ApJ, 516, 604
Iwasawa K., 1999, MNRAS, 302, 96
Iwasawa K., Comastri A., 1998, MNRAS, 297, 1219
Kauffmann G., Haehnelt M., 2000, MNRAS, 311, 576
Lawrence A., Elvis M., Wilkes B. J. et al., 1997, MNRAS, 285, 879
Lawrence A., Rowan-Robinson M., Ellis R. S. et al., 1999, MNRAS, 308, 897
Lipari S., 1994, ApJ, 436, 102
Lipari S., Colina L., Macchetto F., 1994, ApJ, 427, 174
Lutz D., Veilleux S., Genzel R., 1999, ApJ, 517, L13

Magorrian J., Tremaine S., Richstone D. et al., 1998, AJ, 115, 2285
Mamon G. A., 1987, ApJ, 321, 622
Mathews W. G., Brighenti F., 1998, In: D. Zaritsky ed., ASP Conf. Proc. 136, Galactic Halos, 277
Mulchaey J. S., Zabludoff A. I., 1999, ApJ, 514, 133
Ogasaka Y., Inoue H., Brandt W. N. et al., 1997, PASJ, 49, 179
Pappa A., Georgantopoulos I., Stewart G. C., 2000, MNRAS, 314, 589
Ponman T. J., Allen D. J., Jones L. R. et al., 1994, Nature, 369, 462
Ponman T. J., Bourner P. D. J., Ebeling H., Böhringer H., 1996, MNRAS, 283, 690
Reeves J. N., Turner M. J. L., 2000, MNRAS, 316, 234
Rigopoulou D., Lawrence A., Rowan-Robinson M., 1996, MNRAS, 278, 1049
Risaliti G., Gill R., Maiolino R., Salvati M., 2000, A&A, 357, 13
Sanders D. B., Mirabel I. F., 1996, ARA&A, 34, 749
Saunders W., Sutherland W. J., Maddox S. J. et al., 2000, MNRAS, 317, 55
Schmidt M., Green R. F., 1986, ApJ, 305, 68
Schulz H., Komossa S., Greiner J., 1998, A&A, 330, 823
Schweizer F., 1989, Nature, 338, 119
Stark A. A., Gammie C. F., Wilson R. W. et al., 1992, ApJS, 79, 77
Surace J. A., Sanders D. B., ApJ, 512, 162
Surace J. A., Sanders D. B., Evans A. S., 2000, ApJ, 529, 170
Vader J. P., da Costa G. S., Frogel J. A., Heisler C. A., Simon M., 1987, AJ, 94, 847
Vignati P., Molendi S., Matt G. et al., 1999, A&A, 349, L57
Vikhlinin A., Mcnamara B. R., Hornstrup A. et al., 1999, ApJ, 520, L1
Voges W., Aschenbach B., Boller Th. et al., 1999, A&A, 349, 389
Weil M. L., Hernquist L., 1996, ApJ, 460, 101
Wilman R. J., Fabian A. C., Cutri R. M., Crawford C. S., Brandt W. N., 1998, MNRAS, 300, L7
Xia X.-Y., Mao S., Wu H. et al., 1999, A&A, 341, L13
Zezas A. L., Georgantopoulos I., Ward M. J., 1998, MNRAS, 301, 915
Zheng Z., Wu H., Mao S. et al., 1999, A&A, 349, 735